ELSEVIER

Nuclear Instruments and Methods in Physics Research A 463 (2001) 9–25

NUCLEAR INSTRUMENTS & METHODS IN PHYSICS RESEARCH Section A

www.elsevier.nl/locate/nima

Design considerations of 10 kW-scale extreme ultraviolet SASE FEL for lithography

C. Pagani[a], E.L. Saldin[b,*], E.A. Schneidmiller[b], M.V. Yurkov[c]

[a] *INFN Milano-LASA, Via Cervi, 201, 20090 Segrate (MI), Italy*
[b] *Deutches Elektronen Synchrotron (DESY), Building 25F, Notkestr. 85, 22607 Hamburg, Germany*
[c] *Joint Institute for Nuclear Research, Dubna, 141980 Moscow Region, Russia*

Received 29 August 2000; received in revised form 27 October 2000; accepted 21 November 2000

Abstract

The semiconductor industry growth is driven to a large extent by steady advancements in microlithography. According to the newly updated industry roadmap, the 70 nm generation is anticipated to be available in the year 2008. However, the path to get there is not obvious. The problem of construction of Extreme Ultraviolet (EUV) quantum laser for lithography is still unsolved: progress in this field is rather moderate and we cannot expect a significant break through in the near future. Nevertheless, there is clear path for optical lithography to take us to sub-100 nm dimensions. Theoretical and experimental work in free electron laser (FEL) and accelerator physics and technology over the last 10 years has pointed to the possibility of generation of high-power optical beams with laser-like characteristics in the EUV spectral range. Recently, there have been important advances in demonstrating a high-gain self-amplified spontaneous emission (SASE) FEL at 100 nm wavelength (Andruszkov et al., Phys. Rev. Lett. 85 (2000) 3825). In the SASE FEL powerful, coherent radiation is produced by the electron beam during single-pass of the undulator, thus there are no apparent limitations which would prevent operation at very short wavelength range and to increase the average output power of this device up to 10 kW level. The use of superconducting energy-recovery linac could produce a major, cost-effective facility with wall plug power to output optical power efficiency of about 1%. A 10-kW-scale transversely coherent radiation source with narrow bandwidth (0.5%) and variable wavelength could be an excellent tool for manufacturing computer chips with the minimum feature size below 100 nm. All components of the proposed SASE FEL equipment (injector, driver accelerator structure, energy-recovery system, undulator, etc.) have been demonstrated in practice. This is guaranteed success in the time schedule requirement.

PACS: 41.60.Cr; 52.75.M; 42.62.Cf

Keywords: Free electron laser; Superconducting accelerator; Industrial applications

1. Introduction

Free electron lasers possess several excellent features, such as wavelength tunability, high efficiency and high output power. That is why they attract an attention as a potential tool for a very wide range of perspective industrial applications [1]. The most useful frequency ranges for industrial application of FELs are in the UV and VUV. Recently, an industrial FEL project has been launched by a consortium of industrial firms including DuPont, Xerox, and IBM [2,3]. A

*Corresponding author. Tel.: +49-40-8998-2676; fax: +49-40-8998-4705.

E-mail address: saldin@mail.desy.de (E.L. Saldin).

0168-9002/01/$ - see front matter
PII: S0168-9002(01)00206-6

kilowatt-scale UV FEL would demonstrate the technology, and an array of user laboratories would allow development of the prospective industrial applications, such as photo-induced chemistry, isotope separation, and surface processing. One can expect that in the near future FELs might be widely introduced to high-technology industries. In particular, in the next decade lithography might be highly supported by short-wavelength FELs.

Lithography is a process of printing or copying a pattern from a flat surface. In today's semiconductor industry lithography is used to copy patterns for manufacturing nanoelectronic processors and memory devices for modern computer systems. Progress in lithography has reached the level of the gigabit per memory chip. The light source for optical lithography is shifting from mercury-arc lamps to eximer lasers. The most critical layers are printed now with nominally four times reduction cameras, known as "optical steppers", using 193 nm wavelength ArF laser as the source. The stepper involves an illumination system, the mask pattern that is to be replicated, a demagnifying optical system and a photoresist coat to record the demagnified image of the mask pattern. The mask pattern is generated using electron beam lithography. The reduction imaging system permits the printing of patterns with feature size approximately equal to the wavelength.

Moore's Law, postulated in 1965, predicted the exponential increase in the number of devices per chip. The exponential decrease in the minimum feature size (from 10 to 0.18 μm linewidth dimensions) sustained by optical lithography over the past several decades provided exponential increase in the memory chips from 1 kB to 1 GB [4]. Table 1 shows an anticipated future trend in which minimum feature size has to be reduced by $\sqrt{2}$ every 3 years in order to increase the number of devices per unit area by a factor of two. Critical dimensions for use in a high volume manufacturing are to be decreased from 180 nm in the year 1999 to 100 nm in the year 2006, and to 50 nm in the year 2012 [4,5]. At present several approaches, called "Next-Generation Lithographies", are being developed. These approaches are extreme

Table 1
Progress in lithography [5]

Year of first shipment	Minimum feature size (nm)	Memory (bits)
1986	1000	1 M
1988	700	4 M
1990	500	16 M
1994	350	64 M
1997	250	256 M
1999	180	1 G
2002	130	4 G
2005	100	16 G
2008	70	64 G
2011	50	256 G

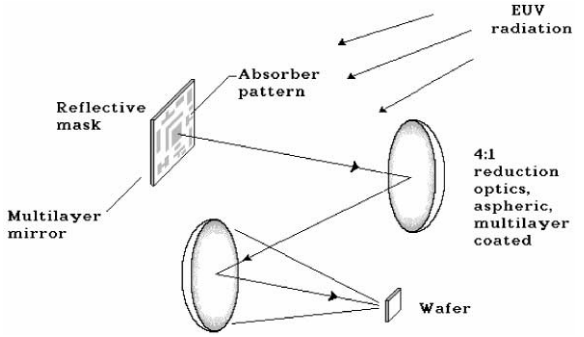

Fig. 1. The basic concept of EUV lithography [5].

ultraviolet lithography (EUVL) [5,6], electron beam lithography [7], X-ray lithography [8], and ion beam lithography. Up to now these investigations passed feasibility study only, and it is not clear when one can expect industrial tool for sub-100 nm lithography.

In this paper we discuss only EUVL approach which can cover the dimension range from 100 nm down to 10 nm. Based on multilayer coated reflective optics, EUVL makes a jump in wavelength to the sub-100 nm region while maintaining the evolution of optical techniques and the industry investment therein. Fig. 1 shows schematically the basic elements of EUV lithography (see Ref. [5]). Transversely coherent radiation illuminates a multilayer coated reflective mask that is overcoated with an absorber pattern. Multilayer coated reduction optics are then used to replicate the pattern at nominal 4:1 reduction on a photoresist-coated wafer. Because multilayer

reflectivities are limited to about 70% in this spectral region, the number of mirrors used is limited by throughput considerations. In order to correct for aberrations across the relatively large field, being limited to a few optical surfaces, one must turn to aspheric optics.[1] The reduction optics must be highly corrected so as to print nearly diffraction-limited patterns at the wafer. This is a new challenge for mirrors and multilayers. It is also necessary to develop the new materials needed for photoresists and photomask.

The new short wavelength light sources must be developed for the EUV lithographic process. Significant efforts of scientists and engineers working in the field of conventional quantum lasers are directed towards the construction of powerful EUV laser for lithography. Nevertheless, this problem is still unsolved. Let us present specific example for modern laser-pumped EUV laser. Recently, there have been important advance in demonstration laser-pumped EUV laser having relatively small scale [9,10]. Paper [10] reports on the first saturated operation of laser-pumped, table-top EUV laser system with the wavelength ranging from 14 to 33 nm. A long-pulse (600 ps FWHM, 1 J energy per pulse) and a short-pulse (1 ps FWHM, 5 J energy per pulse) beam from table-top, 1.053 μm Ti:sapphire–Nd:glass hybrid chirped-pulse amplification laser system are sent into the target chamber. The short pulse is focused onto the target to form an 80 μm × 12.5 mm line focus, while a long pulse is two times broader to ensure a better overlap with the short pulse. The laser system can be fired once every 4 min. The authors of paper [10] have demonstrated a saturated EUV laser at 19 nm with total output energy of up to 2.4 μJ with 7 ps pulse duration and 5 mrad × 10 mrad divergence in a 0.01% bandwidth. The FWHM of the lasing region is about 90 μm × 70 μm. Let us analyze these experimental results. First, we obtain that table-top EUV lasers lack transverse mode control, and substantial spatial filtering is required for applications requiring good spatial coherence (for example, lithography). The coherent power available after spatial filtering can be written as [5]

$$W_{\mathrm{coh}} = \frac{(\lambda/2\pi)^2}{(D_x\theta_x)(D_y\theta_y)} W_{\mathrm{laser}}$$

where W_{laser} is the radiated laser power occupying an elliptical phase-space $(D_x\theta_x)(D_y\theta_y)$. Recalling the EUV table-top laser radiating 300 kW in a single 7 ps pulse at a wavelength of 19 nm, we can now estimate the coherent power that would be available after spatial filtering. With a source diameter $D_x \simeq D_y$ estimated at 100 μm and a divergence half angle $\theta_x \simeq \theta_y$ of 5 mrad, the product $D\theta$ is approximately 200 times larger than $\lambda/2\pi$. The single pulse coherent power available after spatial filtering is therefore about $300\ \mathrm{kW}/(200)^2$, or 7 W. Considering the pulse duration of 7 ps, this corresponds to an energy of 50 pJ at very low repetition rate. In potential, for table-top laser system with 100 Hz repetition rate one can expect an average spatially coherent power of about 10 nW.

Let us proceed with further estimations of using this radiation for lithography process. It is expected that a resist for EUV lithography should be exposed by energy flux of about $10\ \mathrm{mJ/cm^2}$ [11]. This value cannot be made significantly less, since statistical fluctuations due to photon shot noise should be small. A typical EUV camera is composed of at least four multilayer coated mirrors and one reflective mask [6,11]. Typically, reflection coefficient of multilayer mirror is about 70%, so total transmission factor through the EUV camera is about $(0.7)^5 \simeq 0.15$. Thus, we find that the minimum value of spatially coherent radiation energy required for replication of a pattern onto one field of 20 mm × 20 mm dimensions should be about 0.2 J. Typically, production of one chip involves replication of 20–30 patterns which needs at least 5 J of spatially coherent radiation energy from laser. Presently, lithography steppers used in semiconductor industry involve KrF or ArF eximer lasers having an average power of about 10 W. Taking into account these considerations we can state that it would be too optimistic to scale present state of EUV quantum lasers to that needed for industrial applications.

It is worth mentioning that present level of accelerator and free-electron laser technique

[1] That is optics that are designed to have surfaces that depart from spherical.

allows to solve the problem of powerful laser for EUV lithography. FEL is a device in which electromagnetic radiation is amplified by the electron beam moving in the undulator. FEL devices can be divided into two classes: amplifiers and oscillators. FEL amplifier amplifies the input electromagnetic wave from the external master oscillator. The FEL oscillator can be considered as an FEL amplifier with feedback. For an FEL oscillator in the optical wavelength range the feedback is carried out by means of an optical resonator. An attractive feature of the high gain FEL amplifier scheme is the absence of no apparent limitations which would prevent operation at short-wavelength range. Since the amplification process develops in vacuum during one pass of the electron beam through the undulator, the problem of the absorption of the radiation in the cavity mirrors does not exist at all. An important problem is that of input signal. Since the desired wavelength is very short, there is no laser to provide the input electromagnetic wave. Nevertheless, fluctuations of the electron beam current density can serve as the input signal in the FEL amplifier. These fluctuations always exist in the electron beam due to the effect of shot noise. An FEL amplifier which starts up from shot noise is frequently known as a self-amplified spontaneous emission (SASE) FEL. In the SASE FEL lasing occurs in a single pass of a relativistic, high-quality electron bunch through a long undulator magnetic structure. Similar to theory of vacuum-tube devices, it is convenient to introduce the notion of the effective power of the shot noise, W_{sh}, at the entrance of FEL amplifier. Typical parameters for a SASE FEL operating in the EUV wavelength range are: W_{sh} of about a few watts and power gain of SASE FEL at saturation, $G = W_{sat}/W_{sh}$ of about 80 dB. The radiation from SASE FEL is completely polarized and has nearly full transverse coherence. Since the wavelength of a SASE FEL is adjustable, selection of new materials needed for photoresists and photomask may be much easier than for the case of fixed-wavelength lasers.

Recently, there have been important advances in demonstrating a high-gain SASE FEL at 100 nm wavelength [12]. The experimental results presented in Ref. [12] have been achieved at the TESLA Test Facility (TTF) FEL at DESY. The goal of the TTF FEL is to demonstrate SASE FEL emission in the VUV and, in the second phase, to built a VUV–soft X-ray user facility [13,14]. The power gain achieved at the TTF FEL is about 40 dB and is limited by the length of the undulator of 13.5 m. Saturation is expected at the undulator length of about 22 m. Later the TESLA team demonstrated tunability of the SASE FEL in the wavelength range from 80 to 180 nm [15]. Minimal wavelength has been limited by the energy of the accelerator available at that moment. Recently, it has been reported about achievement of the saturation in the SASE FEL at the Argonne National Laboratory operating in the visible wavelength range.[2] Both experimental results are in good agreement with theoretical predictions and form reliable experimental basis for industrial EUV FEL discussed below.

In this paper we present design considerations of a 10-kW-scale SASE FEL based on superconducting RF linear accelerator (SRF accelerator). Typically, only less than one per cent of electron energy is converted to radiation. With SRF linac, a SASE FEL would acquire high average power, owing to the input beam continuous-wave (CW) nature. The energy recovery of most of the driver electron beam energy would increase the power efficiency. The design consists of a 12 MeV electron injector, a one pass 1000 MeV accelerator, and a uniform undulator. The exhaust electron beam from the FEL is decelerated for the energy recovery and dumped at 10 MeV. The stringent electron beam qualities required for EUV SASE FEL operation can be met with a conservative injector design (using a conventional thermionic DC gun and subharmonic bunchers) and the beam compression and linear accelerator technology, recently developed in connection with high-energy linear collider and X-ray FEL programs [16,17]. In our project we use conservative values for a normalized emittance of 8π mm mrad and longitudinal emittance of 300 keV mm at 2 nC

[2] Saturation in the high-gain SASE FEL operating in the visible wavelength range has been achieved at the Argonne National Laboratory. Up-to-date information can be obtained at the web page http;//www.aps.anl.gov.

charge per bunch. Simulations performed in this paper shows that predicted SASE FEL efficiency (i.e. the ratio of the energy in the radiation pulse to the energy in the electron pulse) is about 0.1%.

The SASE FEL described in this paper, provides for the 70 nm wavelength average output optical power up to 10 kW. The radiation from SASE FEL is spatially (or, transversely) coherent. Comparing these parameters with those for the best laser-pumped table-top EUV lasers [9,10] we can expect up to 12 orders of magnitude larger spatially coherent average power. Such an enormous advantage in spatially coherent average power would allow to simplify greatly performance of the EUV stepper. In particular, it is not so necessary to use multilayer mirrors. There are other candidate materials which have the potential to provide more attractive engineering and economical solutions. For instance, silicon carbide (SiC) has a reflectivity at normal incidence of about 40% in the EUV wavelength range between 60 and 100 nm. It can be polished to a supersmooth surface with rms roughness of 2 Å . This material is very hard, stable and has high electrical conductivity and excellent thermal properties, such that surface distortions caused by high average absorbed power are negligible. SiC mirrors with characteristics required for EUV optics are produced by industry and are widely used at synchrotron radiation beam lines. This can be an additional advantage for compressing development time for the EUV lithography.

The paper proceeds as follows. In Section 2 we describe the basic ideas of the proposal. Section 3 is devoted to the description of the accelerator, bunch compressors and the transport optics necessary to produce an electron beam suitable for a high-power EUV SASE FEL. The conceptual design of the high-gain EUV SASE FEL is described in Section 4. A complete description of the SASE FEL process can be performed only with three-dimensional (3-D) time-dependent numerical simulation code. Application of the numerical calculations allows one to describe the general case of the SASE FEL operation, including the case of an arbitrary axial and transverse profile of the electron bunch, the effects of finite pulse duration and nonlinear effects. Optimization of the parameters of the EUV SASE FEL in our case has been performed with the code FAST [18]. We calculate the average radiation power, radiation spectrum envelope, angular distribution of the radiation intensity in far zone.

When considering possible technical realization of injector, driver accelerator structure, undulator and energy recovery system, we have used only those technical solutions which have been used elsewhere. This is guaranteed success in the time schedule requirement (70 nm feature size in the year 2008). The development and test of the tools for the EUV lithography is greatly facilitated by the fact that required parameters of the radiation source are practically identical to those being developed in framework of VUV SASE FEL at the Tesla Test Facility (TTF) at DESY. The SASE FEL at DESY will produce in the wavelength range of 10–70 nm train of 0.5 ps micropulses, with about 1 mJ of optical energy per macropulse at a repetition rate of 9 MHz. The 1000 MeV SRF accelerator will operate at 1% duty factor. The average output EUV optical power can exceed 50–100 W. Commissioning of this facility could start in 2003. The SASE FEL at the TTF would allow to test various novel hardware components and could be used for pilot tests of the sub-100 nm lithography technology.

2. Facility description

Fig. 2 shows the general scheme of the 10-kW-scale EUV SASE FEL. The injector is practically identical to that designed at LBL for the CW-mode operation infrared FEL [19] (see Figs. 3 and 4). The injector consists of a high-voltage DC gun with gridded thermionic cathode and two subharmonic, room-temperature buncher cavities and 500 MHz accelerator buncher cavity. The injector produces electron bunches with energy 6.5 MeV, bunch charge 2 nC, and pulse duration 33 ps (FWHM). Repetition rate of electron bunches is 6.1 MHz and average current produced by the injector is 12.2 mA. A 500 MHz single-cavity cryounit follows the injector which increases the energy of electrons up to 12 MeV. Both 500 MHz cavities operate at an accelerating gradient

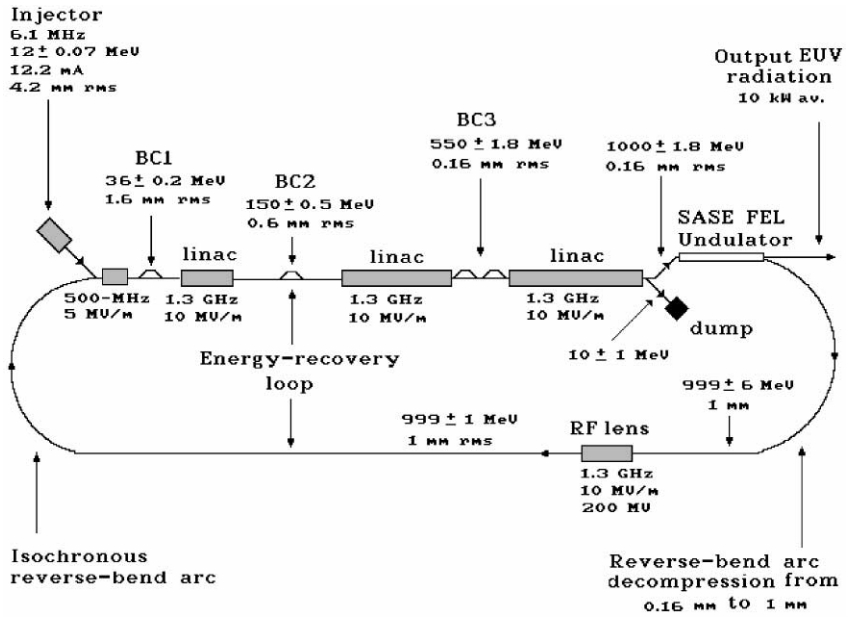

Fig. 2. Basic scheme of the high-power EUV SASE FEL.

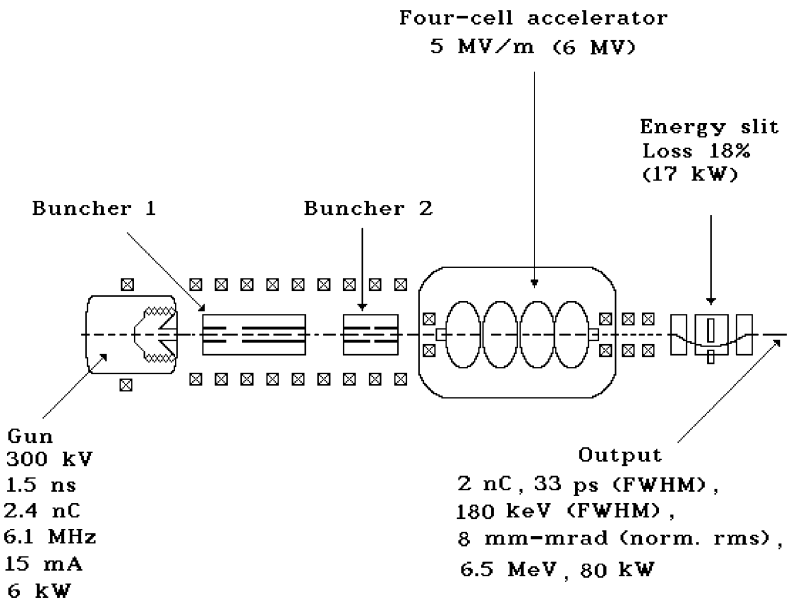

Fig. 3. Layout of the EUV SASE FEL injector.

of 5 MV/m. The low-energy electron beam then enters the SRF linac for further acceleration up to the energy of 1000 MeV. Superconducting cavities of this regular part of the linac are designed to operate at a frequency of 1300 MHz with nominal accelerating gradient of 10 MV/m. 1 GeV electron beam enters the undulator, yields EUV coherent radiation, and finally decelerates through an

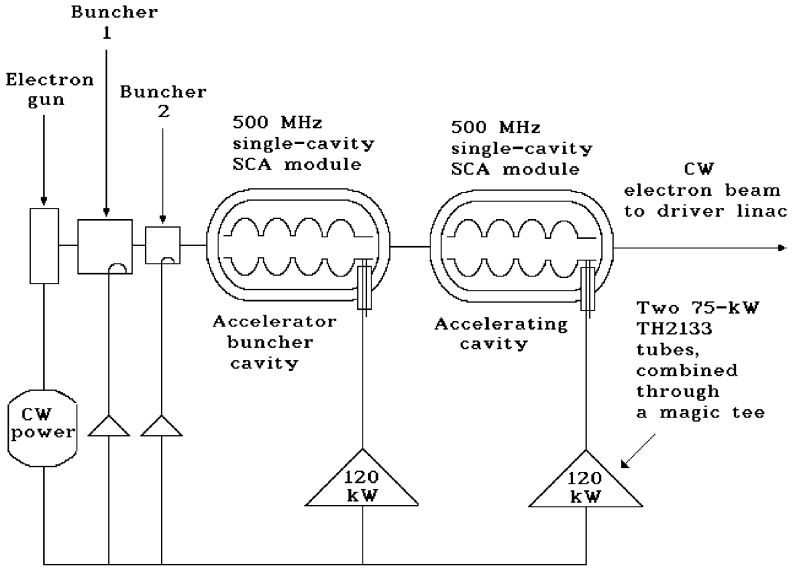

Fig. 4. Schematic of the RF injector system.

energy-recovery pass in the SRF driver linac before its remaining energy is absorbed in the beam dump at the final energy of about 10 MeV. In the present design the beam dump energy is below the photon–neutron production threshold, so the problem of radio-nuclide production in the dump does not exist. The SASE FEL provides a continuous train of 0.5 ps micropulses, with 2 mJ of optical energy per micropulse at a repetition rate of 6.1 MHz. The average radiation output power can exceed 10 kW. The radiation from SASE FEL is spatially (or transversely) coherent. The temporal (or longitudinal) coherence, however, is poor due to the start-up from noise. The bandwidth of the output radiation would be about 0.5% FWHM.

A driver linac design requires considerable manipulation of the longitudinal and transverse beam dynamics in order, on the one side, to provide the bunch parameters for effective generation of the SASE radiation, and on the other side, to make effective energy recovery feasible. A relatively high value of beam peak current is needed in the undulator to reach high gain amplification within a reasonable undulator length. In our design this value is about 1.5 kA, corresponding to 0.16 mm rms bunch length for 2 nC bunch charge. This value is not attainable directly in the injector, because the space charge forces would blow up both the transverse beam size and the energy spread. Thus, the use of magnetic bunch compression at higher energy is foreseen in order to reduce the bunch length. In an ideal bunch compressor, a linear correlation between energy and longitudinal position is induced in the bunch, by passing an RF accelerator structure with off-crest phase. Then there follows a sequence of bending magnets where particles with different energies have different pass lengths. As a result, the bunch tail has a shorter path and can catch up with the head, effectively compressing the bunch. The magnetic bunch compressors are arranged and located such that nonlinearities in the compression and acceleration process (RF curvature, space charge effects, longitudinal wake fields) do not limit the achievable bunch parameters. For the driver accelerator design we assume to use a three-stage compressor design. The compression is performed in three steps: at 36 MeV (from 4.2 to 1.6 mm rms), 150 MeV (from 1.6 to 0.6 mm rms) and 550 MeV (from 0.6 to 0.16 mm rms). Between the first and the second bunch compressor the curvature of the accelerating field would impose an intolerable

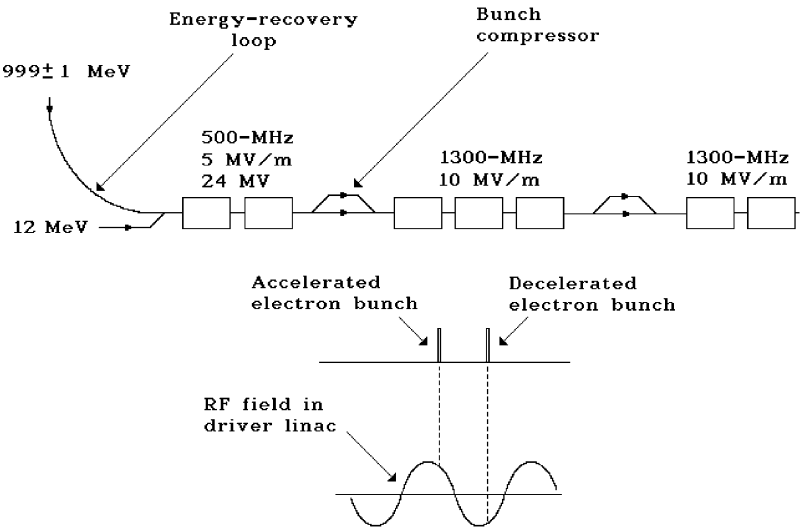

Fig. 5. The scheme of operation of driver linac.

nonlinear correlated energy distribution along the bunch. Thus, the use of the third harmonic deceleration structure is foreseen in order to reduce the nonlinear energy spread.[3] The first (BC1) and the second (BC2) bunch compressors are simple chicanes formed of four rectangular dipole magnets. The third compressor (BC3) is a sequence of two magnetic chicanes. The shorter bunch length and higher energy require for a much longer and more complicated design than BC1 or BC2, and the complexity of double chicane is required [17]. The last part of the driver linac accelerates the bunch with an on-crest phase up to 1000 MeV.

In our conceptual design we assume the use of an energy-recovery system. Only about 0.1% of the electron energy is converted to light. The reminder undergoes energy recovery, being returned to the SRF cavities, where most of it is converted back to RF power at the cavities' resonant frequency. An off-crest deceleration phase should be tuned in order to minimize the RF power consumption by the accelerator (see Fig. 5). The decelerated beam is then dumped. The SRF linac must decelerate the bunches from an energy of about 999 MeV down to about 10 MeV in the beam dump. Here one should take into account an important problem of the induced energy spread in the electron beam at the exit of the SASE FEL which can significantly limit the possibilities of energy recovery. In the present design this problem is solved in the following way. The energy spread of the electron beam after leaving the undulator is pretty large, about $\Delta E \simeq \pm 6$ MeV. An important feature of our design is that a very short electron bunch (of about 0.16 mm rms) is used for the generation of the EUV radiation. Thus, the use of energy bunching is foreseen in order to reduce the energy spread.

Fig. 7 shows the principle of energy compression in the longitudinal phase-space. Energy bunching is appropriate for the situation in which particles are bunched tightly in phase, but have a large energy spread [20]. A similar situation occurs at the undulator exit. The transformations are in the reverse order from those used for phase bunching. A relation is first established between phase and energy, creating a skew "ellipse" in the longitudinal phase space. This is followed by a RF lens that reduces the energy spread by applying a

[3] For our design we had decided to use third harmonic compensator. This solution is based on the need to minimize cost. In order to achieve tolerable value of nonlinear correlated energy spread, without the third harmonic compensator, the beam must be accelerated from 36 to 150 MeV in the 500 MHz accelerator structure.

reverse voltage that returns the "ellipse" to axis. Phase separation (i.e. linear correlation energy and longitudinal position) can be obtained in our case by the first, 180° bend of the recovery loop. Passing this bend, particles with different energies have different pass length mostly because they travel on orbits with different radii through the bending magnets with dispersion. A correlated energy spread in the bunch is cancelled by passing an RF accelerator structure at 90° crossing phase (0° corresponding to running on-crest).

The proposed energy bunching system is sketched in Figs. 6 and 7. After leaving the undulator the beam enters the debuncher. This debuncher is basically part of the first arc transport from the undulator to the driver linac. After leaving the debuncher the bunch length is increased by a factor of 6, and uncorrelated energy spread transforms to the one correlated with the longitudinal position of the particles in the bunch. The shape of the longitudinal density distribution of the bunch is similar to that of the energy distribution. We select 1300 MHz structure for RF lens, based on SRF cavities operating with gradient of 10 MV/m. The transformed phase spread corresponding to this RF frequency is about $\Delta\phi_f = 2\pi\sigma_z/\lambda_{RF} \simeq 0.04$, and ratio $\Delta\phi_f/\Delta\phi_i \simeq 6$. For chosen parameters of the EUV SASE FEL we get induced energy spread $\Delta E_i \simeq 6$ MeV. Voltage V_0 which is sufficient to cancel the 6 MeV energy spread is equal to $V_0 = \Delta E_i/\Delta\phi_f \simeq 200$ MV. The transformed energy spread is about $\Delta E_f = \Delta E_i \Delta\phi_i/\Delta\phi_f \simeq 1$ MeV. It should be noted that in our case the energy bunching can be treated within the framework of single-particle dynamic theory. This situation is in marked contrast to phase bunching, in which the space charge and wake-field effects determine the effective phase-space area occupied by the particles.

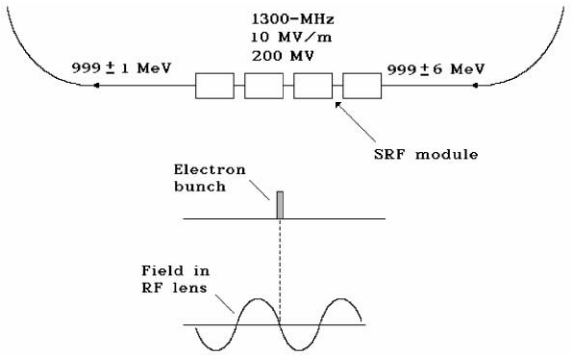

Fig. 6. The scheme of operation of the RF lens.

The wall plug power to output optical power efficiency of SASE FEL for industrial applications

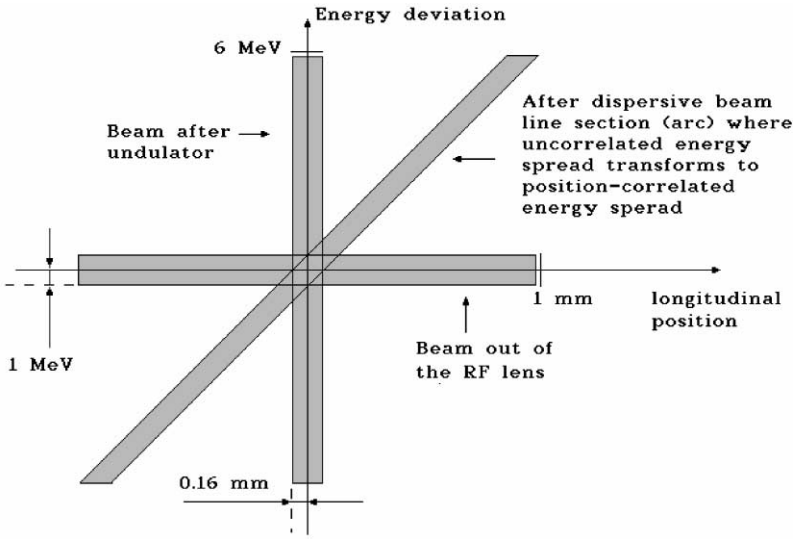

Fig. 7. Principal scheme of bunch compression (linear approximation).

is an important criterion. For the present design we fixed on a rather conservative value of the ratio of the energy in the radiation pulse to the energy in the electron pulse of about 0.1%. Energy recovery of most of the driver electron beam energy would increase the power efficiency and we can reach the RF power to radiation beam power efficiency of about 7%. Assuming the efficiency of the klystron modulator to be 80%, and electronic efficiency of the klystron to be 60%, we obtain that the AC wall plug power to output radiation power efficiency is about 3%. The present design requires cooling of about 25 cryomodules. To do this, we need a He refrigerator with net power consumption of about 1 MW. As a result we obtain total efficiency of proposed SASE FEL about to 1%.

Let us discuss the problem of output optical system for the EUV SASE FEL. Average optical power at the exit of SASE FEL is about 10 kW. To provide the possibility of application for EUV steppers, the laser beam should be divided. In principle, there could be a lot of possibilities to divide initial CW optical beam. Here we consider one of them.

The initial optical beam is transformed into 100 parallel beams of 10 ms macropulse duration and repetition rate of 1 Hz. It could be done, for instance, by means of rotating mirrors. For maximum efficiency the mirrors should be manufactured of highly reflecting material such as SiC. In the range of 50–70 nm the SiC mirror reflectivity at grazing angles 10–15° is about 90% for s-polarization, and 80% for p-polarization. This material has excellent thermal properties such that surface distortions caused by the average absorbed power are negligible. Separation of the optical beams is performed in two steps. At the first step the beam should be divided by the system of 10 rotating mirrors into 10 beams of 10 ms pulse duration and repetition rate of 10 Hz. At the second stage, each of the 10 beams is separated into 10 beams. The radiation power losses in the mirror is about 10%, so integral losses of the radiation power in the dividing system are about 20%, and the output optical system produces 100 laser beams of 80 W average power (macropulse duration 10 ms, macropulse energy 80 J, repetition rate 1 Hz) which are directed to the EUV steppers.

3. Accelerator systems

3.1. Injector system

The design goals for the EUV SASE FEL injector require electron bunches of 2 nC delivered at 6.1 MHz repetition rate, for an average beam current of 12.2 mA. This precludes the use of RF guns using room-temperature RF systems, since these structures in CW operation cannot support the high fields required to deliver the necessary bunch charge within the specified transverse and longitudinal emittances (a superconducting RF gun has been demonstrated, but this technology is insufficiently mature). The arrangement of the injector is shown schematically in Fig. 3. Our design is practically identical to that of LBL developed for the CW-mode operation infrared FEL oscillator [19]. The injector starts with DC grid-controlled thermionic gun as a source. The gun operates at a voltage of 300 kV and produces 2.4 nC pulses with a duration of 1.5 ns (FWHM). A 2 cm^2 thermionic cathode provides the needed current. The bunch compression is performed by means of a sequence of three bunchers operating at fundamental frequencies of 61, 171 and 500 MHz. The 500 MHz buncher is a superconducting structure and the other two operate at room temperature. Both subharmonic bunching cavities use quarter-wavelength coaxial cavities operating at the fundamental TEM-mode. An appropriate SRF structure is 500 MHz four-cell structure manufactured by Dornier for the HERA storage ring at DESY. We also adopted the gradient 5 MV/m for the present design. Details regarding bunchers design and their operating parameters can be found in Ref. [19]. A chicane with a high-power energy slit capable of a scraping up to 17 kW, or 18% of the beam is needed between the injector and accelerator. The slit removes electrons in the tail of the spectrum more than 90 keV below the mean of the energy distribution. The slit is approximately 1 m long, the power density will remain everywhere well below the 500 W/cm^2 limit. Local X-ray shielding will be provided, but the 6 MeV beam will produce no neutrons and no component activation. The injector is followed by a 500 MHz single-cavity superconducting accel-

erator module which increases the beam energy to 12 MeV. This cryounit might be considered as a part of the injector. The optimized beam parameters at the exit of the cryounit are: bunch charge 2 nC, bunch length 4.2 mm rms, normalized transverse emittance 8π mm mrad, and longitudinal rms emittance 300π keV mm. Accelerator buncher cavity and first accelerating cavity operating without energy recovery, will require about 170 kW RF power. The klystrons are two 75 kW TH2133 tubes, combined through a magic tee to provide the 120 kW of RF at the input coupler to each cryounit (see Fig. 4). Results of stability analysis of the injector are presented in Ref. [19]. The charge stability $<2\%$, bunch length stability $<2\%$, and bunch timing stability <3 ps are well within RF control system capability.

3.2. Driver accelerator system

For the driver accelerator we select 1300 MHz structure, based on a standing-wave superconducting cavities with the gradient of 10 MV/m. The accelerator consists of 20 SRF modules with total voltage of 1000 MV similar to CEBAFs two 20-module linacs. Each cryomodule contains eight nine-cell π-mode cavities. Each cavity has an input coupler for RF power. For our design we had decided to power each cavity by one QKW1750 tube from Raytheon. The eight tubes powering the eight cryomodule cavities can each deliver up to 1.5 kW. This level is comparable to that demonstrated at CEBAF. RF power limits the CW average current to a maximum of 0.3 mA in the straight-ahead mode. However, if the energy recovery is established, the decelerated beam powers the accelerated beam, thus increasing the average current up to 12 mA, limited by the injector.

For RF curvature compensator (see Section 2) we select 3.05 GHz structure (500×6.1 MHz), based on a standing-wave superconducting cavities with the gradient of 5 MV/m. The compensator consists of one cryomodule with total voltage of 15 MV similar to the TTF RF curvature compensator which is planned to be installed at DESY. The cryomodule contains four cavities. We had decided to power each cavity by one 1 kW TH2047 tube from Thomson. This is conventional CW klystron used in radars.

The RF lens consists of four 1300 MHz superconducting accelerating modules with total voltage $V_0 \simeq 200$ MV. Electron beam passes the RF lens at 90°-crossing phase, so this RF structure is passive. Thus, each cryomodule of RF lens will use one 1.5 kW QKW1750 tube. RF control of superconducting linac used by CEBAF demonstrated stability at the level of 5×10^{-5} in the amplitude and 0.1° in phase. For our design we have adopted the CEBAF RF feedback system.

3.3. Bunch compressors

A bunch compressor can be constructed from an RF section introducing a $\delta E - z$ correlation and a bending system (magnetic chicane) where the pass length is energy dependent. Finally, the compressed bunch length and energy are given by

$$z_f = z_i(1 + kR_{56}) + R_{56}\delta E_i/E_f$$

$$\delta E_f/E_f = kz_i + \delta E_i/E_f$$

where

$$k = \frac{d(\delta E)}{E_f dz} = \frac{eV_0 k_{RF} \sin\phi}{E_i + eV_0 \cos\phi}.$$

Here $\delta E_i/E_f$ represents small injection energy deviations scaled to the final energy, R_{56} is the $(5,6)$ element in the linear transfer matrix, V_0 is the RF voltage, $k_{RF} = 2\pi/\lambda_{RF}$ is the RF wavenumber, and ϕ is the RF phase where 0° corresponds to running on the RF crest. For full compression the parameters are chosen so that $k = -1/R_{56}$. In this case the R_{56} is determined by the initial energy spread and the desired bunch length.

The proposed phase bunching system is sketched in Fig. 2. The first compression is from 4.2 to 1.6 mm rms. The second stage consists of three 50 MV SRF modules followed by a magnetic chicane generating the R_{56} needed for bunch compression. First 5 m long chicane contains four C-type bending magnets with a gap width of 3 cm. The bending magnets are rectangular magnets which do not have net focusing in the horizontal plane and do not generate higher order dispersion.

Chicane generates $R_{56} \simeq 10$–20 cm at deflection angle of 10–20° [21].

Bunch compression will be done in stages to avoid space charge and coherent synchrotron radiation (CSR) effects limiting the achievable bunch length and transverse emittance. Calculation of the space charge forces in a bunched beam shows that this should not be a serious limitation in our case. In contrast, the electric field of the CSR induces an energy variation along the bunch, i.e. the CSR field is similar to a longitudinal wake field. In the chicane, this field will destroy the achromaticity of the compressor and the horizontal emittance will be increased. If we neglect the shielding effects of the vacuum chamber, the CSR induced energy spread is predicted to be roughly [22]

$$\delta E/E \simeq 0.2 N_e r_e L_B/(\gamma R^{2/3}\sigma_z^{4/3})$$

where L_B and R are the bending magnet length and bending radius, and r_e and γ are the classical electron radius and the relativistic factor. Since the bunch length shortens through the chicane, the energy spread induced at each dipole increases with the final dipole generating the most significant energy spread (the bunch length is virtually constant in the first and last dipole). The emittance growth for just the last bend of a single chicane is [17]

$$\gamma\Delta\varepsilon_{CSR} \simeq 0.16 r_e N_e \left(\frac{\theta_B^5 L_B}{\sigma_z^4}\right)^{1/3} \times \sqrt{\frac{\varepsilon_n}{\gamma}\left(\frac{L_B^2}{9\beta} - \frac{L_B}{3} + \frac{\beta}{2}\right)}$$

where $\Delta\varepsilon_{CSR}$ adds in quadrature to the initial emittance, ε_n is the normalized initial emittance, θ_B is the bend angle, β is beta-function. The CSR is suppressed by vacuum chamber. The point where shielding becomes important can be estimated as $\sigma_z > h^{3/2}/R^{1/2}$, where h is the transverse size of the chamber. In the second bunch compressor (BC2), we find that shielding is important and the CSR induced energy spread will be significantly reduced. Calculation of the CSR effects with shielding shows that induced energy spread and emittance dilution should not be a serious limitation in BC2.

After leaving the second bunch compressor electron bunch of 0.6 mm (rms) length is accelerated in the next part of the driver linac from an energy of 150 to 550 MeV. For the third compression stage the required large correlated energy spread in the bunch of 2 MeV rms is induced by passing the second part of the linac (having voltage $V_0 \simeq 500$ MV) at 15° crossing phase. Finally, the electron bunch is compressed from 0.6 to 0.16 mm in the third bunch compressor (BC3). The shorter bunch length and higher energy allow for a much longer and more complicated design than BC2 and the complexity of double chicane is required [17].

Requirements for magnetic bunch compressors in our case are very close to those for magnetic bunch compressors in X-ray FELs [13,14,16,17]. In particular, the magnetic chicanes for the soft X-ray SASE FEL at DESY, which is presently under construction, is a good example for many problems related to our bunch compressor design [21]. The first TTF bunch compressor is located after the 150 MeV acceleration section and compresses the bunch with $\sigma_z \simeq 1.6$ to 0.3 mm. In the second stage the bunch is compressed to the final length of $\sigma_z \simeq 50$ μm at the energy of 500 MeV. Analysis of parameters of an X-ray SASE FEL at TTF shows that the energy of the bunch in the compressors and values of R_{56} are close to those required in our design. This equality of R_{56} is a consequence of the fact that the final TTF bunch length ($\sigma_z \simeq 50$ μm at 1 nC charge per bunch) is three times smaller compared to our design ($\sigma_z \simeq 160$ μm at 2 nC bunch charge per bunch), but final energy spread at TTF is two times smaller, too. Comparing parameters of the TTF with our design we can conclude that to make preservation of the transverse emittance in the case of the TTF parameters is more difficult. On the one hand, normalized transverse emittance ($\varepsilon_n \simeq 2\pi$ mm mrad) is significantly less compared to our design ($\varepsilon_n \simeq 8\pi$ mm mrad). On the other hand, in our case the peak current is about 1.5 times smaller and the bunch length about three times larger. Thus, the predicted CSR induced energy spread and emittance dilution at the TTF are larger compared to our design. This means that successful operation of the TTF will prove that

high-quality electron bunches with peak current of about 1.5 kA might be obtainable, and there is no need to build a special bunch compression facility for verifying the proof-of principle.

3.4. Electron beam transport

The beam will be recirculated through two 180° arcs for further deceleration in the same SRF structures, to a minimum energy of about 10 MeV. In the undulator, the energy spread in the beam is increased in the process of the FEL interaction, to as much as $\Delta E_i \simeq \pm 6$ MeV. The first arc transport from the undulator to the driver linac is nonisochronous and is optimized for an effective bunch decompression. After passing this arc, the beam bunch is lengthened, and position of the particle along the bunch becomes correlated with the energy, i.e. we have the energy tilt along the bunch. Tilt is then removed in RF lens, where energy spread is reduced to $\Delta E_f \simeq \pm 1$ MeV. The RF lens consists of a 1300 MHz SRF structure that provides a total voltage of 200 MV, and operates at the phase of $\phi_0 = 90°$. The first arc performs a decompression to the bunch length of $\sigma_z \simeq 1$ mm. In the linearized limit, this implies: $R_{56}\Delta E_i/E \simeq 0.1$ cm, or $R_{56} \simeq 15$ cm. The quantity of R_{56} is naturally about few meters in a typical arc transport at this energy. In our case we desire it to be much smaller. To obtain the desired value of R_{56}, the lattice of the arc must be perturbed with the introduction, for example, of negative bends. In addition to R_{56} control, the arc transport must be achromatic. A compact nearly-isochronous lattice can be obtained using a "reverse-bend"-type lattice, originally developed in Ref. [23] and used at the DEMO facility [24]. This lattice consists of achromatic cells, each of which consists of a large positive bend, a set of matching quadrupoles, and a negative bend, followed by mirror image set of matching quadrupoles and positive bend. The combination of small dispersion (η) at the large bends and large tunable η at small negative bends leads to nearly zero value of R_{56}.

Energy-recovery linac can, in principle, exhibit instabilities in the beam energy. These instabilities arise from fluctuations of the cavity fields. Coupling from the beam energy to the current and phase is included via beam loss on aperture (scraping) and nonzero compaction factor. Both effects change the beam-induced voltage in the cavities. Depending on the RF feedback characteristics, this can lead to the instabilities in the accelerating field. Stability analysis of the SRF energy-recovery linac with CEBAF feedback system (which we have adopted in our design) has been performed in Ref. [25]. It was found that, for small variations, modest gain frequency, well within CEBAF RF control system capability, is required to stabilize the system. Recently, according to the schedule of Phase I, Jefferson Laboratory energy-recovery SRF linac has exceeded design specifications. It achieved 48 MeV of beam energy with 4 mA of average beam current [26]. No signature of longitudinal instabilities was observed, in agreement with the modelling predictions [27].

4. The undulator

The undulator is one of the central components of the EUV SASE FEL. It has two functions. First, it has to provide the sinusoidal field, so that the FEL process can take place. Second, additional focussing is required in order to keep the beam size small over the whole undulator length. In our case the undulator is a fixed 11 mm gap permanent magnet device using a combined function magnet design [28] with a period length of $\lambda_w = 45$ mm and a peak field of $B_w = 1.1$ T, resulting in an undulator parameter of $K = 5.5$. The vacuum chamber diameter in the undulator (9 mm) is much larger than the beam diameter (300 μm). Integrated quadrupole structures produce a gradient of 18 T/m superimposed on the periodic undulator field in order to focus the electron beam along the undulator. The undulator system is subdivided into segments, each 4.5 m long and containing 12 quadrupole sections to build up six full focusing–defocusing (FODO) cells. The FODO lattice periodicity runs smoothly from segment to segment. There is a spacing of 0.3 m between adjacent segments for diagnostics. The total length of the system is 22.5 m. For

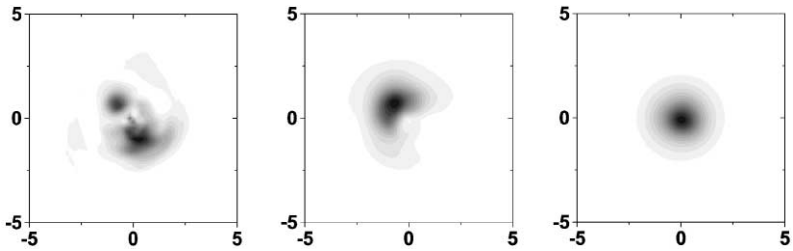

Fig. 8. Distributions of the radiation intensity across one slice of the radiation pulse at different undulator lengths, $z = 8$, 16 and 24 m (left, middle, and right plots, respectively).

optimum overlap the electron and radiation beams high precision on the magnetic fields and mechanical alignment are required. The beam orbit straightness in the undulator is determined by the alignment precision of the superimposed permanent magnet quadrupole fields which is better than 50 μm in both vertical and horizontal directions.

Requirements for this device in our case are close to the undulators in VUV and X-ray FELs [13,14,16,17]. In particular, the 14 m long undulator for the VUV FEL at the TTF, which is presently installed, is a good working example for many problems related to our undulator design [29,30]. It should be noted that VUV SASE FEL undulator at the TTF has the same parameters of strong focusing system.

5. Properties of output radiation

A complete description of the SASE FEL can be performed only with 3-D time-dependent numerical simulation code. Application of the numerical calculations allows one to describe the general case of the SASE FEL operation, including the case of an arbitrary axial and transverse profile of the electron bunch, the effects of finite pulse duration and nonlinear effects. With the framework of design and construction of VUV and X-ray SASE FELs, several 3-D time-dependent codes (GINGER [31], GENESIS [32], and FAST [18]) have been developed in order to describe FEL amplifier start-up from shot noise. Optimization of the parameters of the EUV SASE FEL in our case has been performed with the code FAST. Recently, the reliability of this code has been demonstrated by means of the numerical simulation of the high-gain SASE FEL [12,33].

Fluctuations of the electron beam current density serve as the input signal in the SASE FEL. These fluctuations always exist in the electron beam due to the effect of shot noise. The actual physical picture of start-up from noise should take into account that the fluctuations of the current density in the electron beam are uncorrelated not only in the time but in space, too. Thus, a large number of transverse radiation modes are excited when the electron beam enters the undulator. These radiation modes have different growth rates. During the amplification process, the number of transverse modes decreases. Also, the divergence of radiation beam in the far zone decreases. For sufficiently long undulator the fundamental mode, which has maximal gain, should survive. Information on the transverse coherence formation can be obtained with 3-D time-dependent numerical simulation code. Analysis of simulation results allows us to find the region of parameters when the transverse coherence of the radiation is settled. In Fig. 8 we illustrate the formation of transverse coherence. It is clearly seen how an initially irregular intensity distribution across one slice of the radiation pulse transforms to that corresponding to the fundamental TEM_{00} mode.

The optimized parameters of the EUV SASE FEL are presented in Table 2. Calculations for the SASE FEL require us to perform a large number of statistically independent simulation runs. At the next stage of the numerical experiment the data

Table 2
Performance characteristics of the EUV SASE FEL

Parameter	
Electron beam	
Energy, MeV	1000
rms energy spread, %	0.18
Normalized emittance, π mm-mrad	8
Bunch charge, nC	2
rms bunch length, mm	0.16
Repetition rate, MHz	6.1
Undulator	
Type	planar, Nd–Fe–B/steel
Period, cm	4.5
Gap, mm	11
Maximum peak field, kG	11
External beta-function, cm	100
Number of undulator periods	700
Output radiation	
Wavelength, nm	70
Micropulse duration, ps (FWHM)	0.5
Spectrum width, % (FWHM)	0.5
Micropulse energy, mJ	2
Peak power, GW	3
Repetition rate, MHz	6.1
Average power, kW	12

arrays are handled with post-processor codes to extract different statistical properties of the SASE FEL radiation. Averaging over 100 simulation runs with statistically independent shot noise in the electron beam gives the radiation pulse shape, which is plotted in Fig. 9. We obtain that the duration of the radiation pulse is about 0.5 ps. Numerical simulation code produces an array containing values for the radiation field in the near zone. Integral spectrum of the radiation pulse can be calculated in the following way. Using the values of radiation field in the near zone, we find the radiation field propagating at any angle in the far zone. At the next step of calculations we find the spectral distribution of the radiation power for each angle, and after integrating over all angles we obtain integral spectrum of the radiation pulse. Fig. 10 present the spectrum of EUV SASE FEL operating in the nonlinear regime. The line is the results of the direct averaging of the spectra for 100 pulses. The average transverse distribution of the radiation intensity at the exit of undulator is

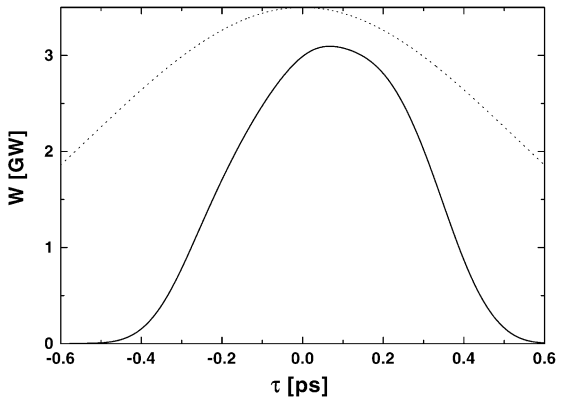

Fig. 9. Typical temporal structure of the radiation pulse at the undulator length of 34 m. Smooth curve is the radiation pulse profile averaged over large number of statistically independent runs. The dashed line presents the longitudinal profile of the electron beam current.

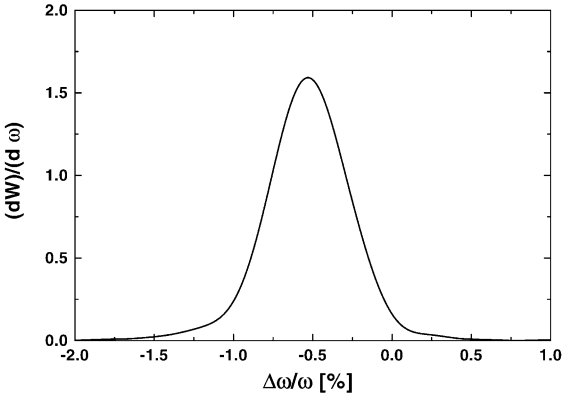

Fig. 10. Typical spectral distribution of the energy in one radiation pulse.

presented in Fig. 11. Fig. 12 shows averaged angular distribution of the radiation intensity in the far zone. An important characteristic of the radiation source is the degree of transverse coherence. Corresponding definitions for the degree of coherence in the high-gain linear regime of the SASE FEL can be found in Ref. [34]. Our simulations show that the degree of coherence in our case is close to unity ($\zeta \simeq 0.9$).

Energy-recovery system will be driven by the spent electron beam leaving the SASE FEL. The SASE process in the undulator induces an additional energy spread in the electron beam. Fig. 13

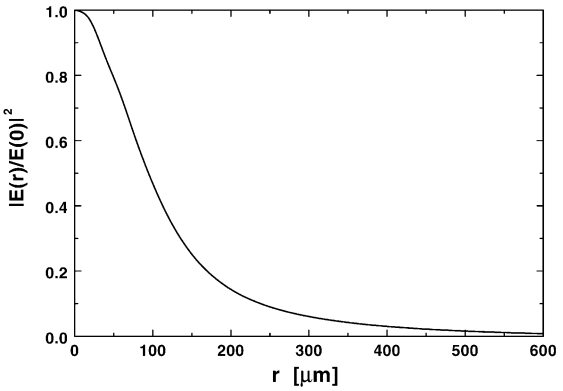

Fig. 11. Radial distribution of the radiation intensity at the undulator length of 34 m averaged over radiation pulse.

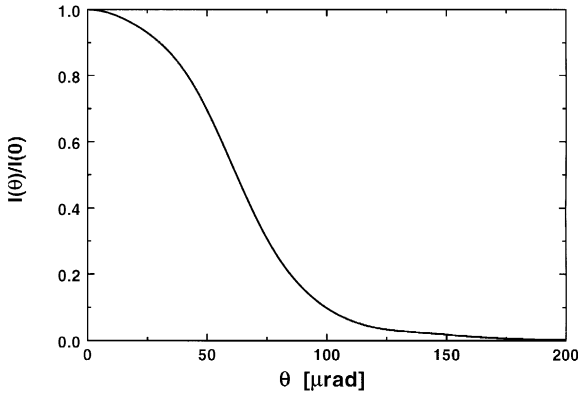

Fig. 12. Angular distribution of the radiation intensity in the far zone at the undulator length of 34 m averaged over radiation pulse.

shows the energy distribution in the electron beam after leaving the FEL undulator. Calculations show that the rms deviation of the energy in the spent electron beam is about $\Delta E \simeq 6$ MeV.

6. Concluding remarks

The frequency choice for the driver accelerator was based on the following considerations. Low RF frequency implies large transverse dimensions and larger cavity volume. Thus, the cavity stores more energy, relative to the beam, and wake-field effects are minimized—both of which improve stability. Cavities in the 352–500 MHz frequency

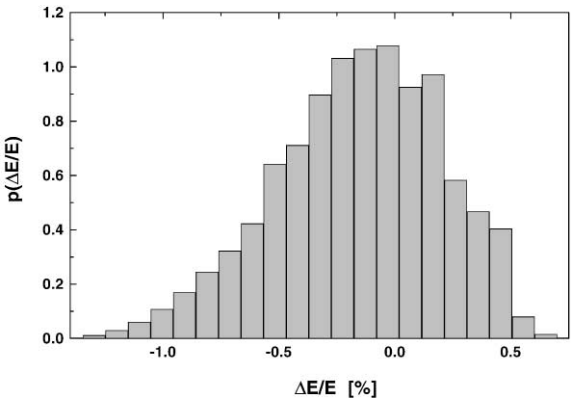

Fig. 13. Energy distribution in the electron beam at the exit of the undulator.

range are in use in the electron–positron storage rings. Their large size is advantageous to suppress wake-field effects and higher order mode (HOM) losses. On the other hand, for the main accelerator the niobium and cryostat costs for the 352 and 500 MHz cavities are prohibitive. In addition, at a higher frequency cryogenic losses are lower. Hence, a higher frequency has been chosen for our design. The value of 1.3 GHz was chosen since the SRF structure with this frequency has been developed at DESY within the framework of the TESLA collaboration. The CEBAF experience with 1.5 GHz SRF structure is of great relevance for our proposal, too, since the cavities are based on the same fabrication techniques.

A possible alternative to frequency 1.3 GHz (or 1.5 GHz) for our proposal could be the frequency 352 MHz. The largest 352 MHz SRF system presently in operation is RF system in storage ring LEP at CERN. A total of 272 four-cell cavities were installed. The SRF modules for this machine have been produced by industry. A 352 MHz LEP structure is advantageous for compressing development time.

Analysis of parameters of a high-power EUV SASE FEL shows that its radiation wavelength range is clearly limited by the quality of the electron beam achievable with injector. Decreasing the radiation wavelength also decreases the maximum tolerable transverse and longitudinal beam emittances. Thus, improving the driver linac injector towards even smaller beam emittances

will be an issue for any radiation frequency upgrade. When considering a possible technical realization of the injector we have used only those technical solutions which have been used 10 years ago. The injector design is based on a conventional thermionic cathode, subharmonic bunchers, and 5 00 MHz cryounit. Even with this technology it is possible to exceed 10 kW level average output power at 70 nm radiation wavelength.

In the following we will sketch some perspectives for the injector upgrade. To obtain a high-quality electron beam without injector scheme modification, a higher DC gun voltage, higher solenoid field and higher gradient in injector cryounit can be chosen for our design. First, it should be noted that DC gun voltage of 500–600 kV is within reach. For example, 10 years ago TRW has built and tested a gun that runs at 500 kV with the required bunch format [35]. Second, the field of superconducting RF structure design is moving forward rapidly, and a gradient of 5 MV/m for four-cell injector cryounit is now considered as a routine. Several manufacturers currently produce superconductive cavities (DESY, CERN, CEBAF), and most will guarantee performance at 10–12 MV/m. As a result the injector will produce electron beam emittance sufficiently low to meet the constraints implied by EUV SASE FEL operating at 50 nm radiation wavelength. For a 10-kW-scale EUV SASE FEL operating in the 10–20 nm wavelength range a new approach for the injector has to be considered. In this context, R&D work on SRF photoinjector [36,37] looks very promising.

Acknowledgements

We thank J.R. Schneider, D. Trines and J. Rossbach for their interest in this work.

References

[1] C. Yamanaka, Nucl. Instr. and Meth. A 318 (1992) 1.
[2] G.R. Neil et al., Nucl. Instr. and Meth. A 358 (1995) 159.
[3] S.V. Benson et al., Nucl. Instr. and Meth. A 429 (1999) 27.
[4] C.P. Ausschnitt, Microelectron. Eng. 41/42 (1998) 41.
[5] D. Attwood, Soft X-rays and Extreme Ultraviolet Radiation, Cambridge University Press, Cambridge, 1999.
[6] R.H. Stulen, D.W. Sweeney, IEEE J. Quantum Electron. 35 (1999) 694.
[7] L.R. Harriot, J. Vac. Sci. Technol. B 15 (1997) 2130.
[8] J.P Silverman, J. Vac. Sci. Technol. B 15 (1997) 2117.
[9] J. Dunn et al., Phys. Rev. Lett. 84 (2000) 4834.
[10] Y. Li et al., J. Opt. Soc. Am. B 17 (2000) 1098.
[11] J.E. Bjorkholm, Intel Technol. J. Q3 (1998) 1.
[12] J. Andruszkov et al., Phys. Rev. Lett. 85 (2000) 3825.
[13] A VUV Free Electron Laser at the TESLA Test Facility: Conceptual Design Report, DESY Print TESLA-FEL 95-03, Hamburg, DESY, 1995.
[14] J. Rossbach, Nucl. Instr. and Meth. A 375 (1996) 269.
[15] J. Rossbach, Proceedings of EPAC2000 Conference, Vienna, Austria, June 2000, p. 88.
[16] R. Brinkmann et al. (Eds.), Conceptual Design of 500 GeV e^+e^- Linear Collider with Integrated X-ray Facility, DESY 1997-048, ECFA 1997-182, Hamburg, May 1997.
[17] The Linac Coherent Light Source (LCLS) Design Study Report, SLAC-R-521, 1998.
[18] E.L. Saldin, E.A. Schneidmiller, M.V. Yurkov, Nucl. Instr. and Meth. A 429 (1999) 233.
[19] K.-J. Kim et al., LBL preprint Pub-5335, 1992.
[20] A.J. Lichtenberg, Phase-Space Dynamics of Particles, Wiley Inc., New York, London, Sydney, Toronto, 1969.
[21] T. Limberg et al., Nucl. Instr. and Meth. A 375 (1996) 322.
[22] Ya. Derbenev et al., DESY print TESLA-FEL 95-05, Hamburg, 1995.
[23] A. Amiry, C. Pellegrini, Proceedings of the Workshop on Fourth Generation Light Sources, SSRL92/02, 1992.
[24] D. Neuffer et al., Nucl. Instr. and Meth. A 375 (1996) 123.
[25] L. Merminga et al., Nucl. Instr. and Meth. A 429 (1999) 58.
[26] G.R. Neil et al., Nucl. Instr. and Meth. A 445 (2000) 192.
[27] L. Merminga et al., Proceedings of the Twenty-first International Free Electron Laser Conference (ISBN 0-444-50481-8) II-3.
[28] J. Pfluger, Y.M. Nikitina, Nucl. Instr. and Meth. A 381 (1996) 554.
[29] B. Faatz, J. Pfluger, Y.M. Nikitina, Nucl. Instr. and Meth. A 393 (1997) 380.
[30] J. Pfluger, H. Lu, T. Teichmann, Nucl. Instr. and Meth. A 429 (1999) 386.
[31] R.A. Jong, W.M. Fawley, E.T. Scharlemann, SPIE 1045 (1989) 18.
[32] S. Reiche, Nucl. Instr. and Meth. A 429 (1999) 243.
[33] E.L. Saldin, E.A. Schneidmiller, M.V. Yurkov, Nucl. Instr. and Meth. A 429 (1999) 197.
[34] E.L. Saldin, E.A. Schneidmiller, M.V. Yurkov, The Physics of Free Electron Lasers, Springer, Berlin, Heidelberg, New York, 1999.
[35] N.H. Lazar et al., Nucl. Instr. and Meth. A 304 (1991) 243.
[36] D. Jansen et al., Conference Proceedings of Particle Acc. Conference, Vancouver, Canada, 1997.
[37] F. Gabriel et al., Nucl. Instr. and Meth. A 429 (1999) II 91.